The Astrophysical Journal, 741:34 (13pp), 2011 November 1 doi:10.1088/0004-637X/741/1/34

ARRIVAL TIME CALCULATION FOR INTERPLANETARY CORONAL MASS EJECTIONS WITH CIRCULAR FRONTS AND APPLICATION TO *STEREO* OBSERVATIONS OF THE 2009 FEBRUARY 13 ERUPTION

C. Möstl[1,2], T. Rollett[1,2], N. Lugaz[3], C. J. Farrugia[4], J. A. Davies[5], M. Temmer[1,2], A. M. Veronig[1], R. A. Harrison[5], S. Crothers[5], J. G. Luhmann[6], A. B. Galvin[4], T. L. Zhang[2], W. Baumjohann[2], and H. K. Biernat[1,2]
[1] Institute of Physics, University of Graz, Graz A-8010, Austria; christian.moestl@uni-graz.at
[2] Space Research Institute, Austrian Academy of Sciences, Graz A-8042, Austria
[3] Institute for Astronomy, University of Hawaii, Honolulu, HI 96822, USA
[4] Space Science Center and Department of Physics, University of New Hampshire, Durham, NH 03824, USA
[5] RAL Space, Harwell Oxford, Didcot OX11 0QX, UK
[6] Space Sciences Laboratory, University of California, Berkeley, CA 94720, USA
Received 2011 May 18; accepted 2011 July 28; published 2011 October 12

ABSTRACT

One of the goals of the NASA *Solar TErestrial RElations Observatory* (*STEREO*) mission is to study the feasibility of forecasting the direction, arrival time, and internal structure of solar coronal mass ejections (CMEs) from a vantage point outside the Sun–Earth line. Through a case study, we discuss the arrival time calculation of interplanetary CMEs (ICMEs) in the ecliptic plane using data from *STEREO*/*SECCHI* at large elongations from the Sun in combination with different geometric assumptions about the ICME front shape [fixed-Φ (FP): a point and harmonic mean (HM): a circle]. These forecasting techniques use single-spacecraft imaging data and are based on the assumption of constant velocity and direction. We show that for the slow (350 km s^{-1}) ICME on 2009 February 13–18, observed at quadrature by the two *STEREO* spacecraft, the results for the arrival time given by the HM approximation are more accurate by 12 hr than those for FP in comparison to in situ observations of solar wind plasma and magnetic field parameters by *STEREO*/*IMPACT*/*PLASTIC*, and by 6 hr for the arrival time at *Venus Express* (*MAG*). We propose that the improvement is directly related to the ICME front shape being more accurately described by HM for an ICME with a low inclination of its symmetry axis to the ecliptic. In this case, the ICME has to be tracked to $>30^\circ$ elongation to obtain arrival time errors $<\pm$ 5 hr. A newly derived formula for calculating arrival times with the HM method is also useful for a triangulation technique assuming the same geometry.

Key words: methods: analytical – solar–terrestrial relations – Sun: coronal mass ejections (CMEs)

Online-only material: animation, color figures

1. INTRODUCTION

Coronal mass ejections (CMEs) are episodic expulsions of huge amounts of plasma and magnetic fields from the solar corona (e.g., Howard et al. 1985). CMEs form a centerpiece of space weather research since they are the source of the strongest disturbances in the Earth's magnetosphere (e.g., Tsurutani et al. 1988; Farrugia et al. 1993; Gosling 1993; Bothmer & Zhukov 2006; Zhang et al. 2007). In addition to other detrimental effects, the resulting geomagnetic storms can knock out communication satellites, lead to errors in global positioning systems, and induce currents on the ground leading to wide-spread electricity blackouts (e.g., report by the Committee on the Societal and Economic Impacts of Severe Space Weather Events 2008). The NASA *Solar TErestrial RElations Observatory* (*STEREO*) mission (Kaiser et al. 2008) was launched in 2006 October and is designed to enhance our understanding of the initiation and propagation of CMEs and thus foster our ability to forecast them using simultaneous imaging in EUV and white-light coronagraphs (Howard et al. 2008), and by sampling the solar wind magnetic fields and plasma using the in situ instruments *PLASTIC* (Galvin et al. 2008) and *IMPACT* (Luhmann et al. 2008). In addition to the three novel viewpoints through in situ instruments and coronagraphs (including *SOHO*/LASCO and the *Wind*/*ACE* in situ measurements near Earth), both *STEREO* spacecraft are equipped with Heliospheric imagers (HIs; Eyles et al. 2009) that can directly map the complete evolution of Earth-directed transients (such as ICMEs) in the inner heliosphere (<1 AU) from a vantage point away from the Sun–Earth line. By definition, we use the term ICME for the structure after it has left any coronagraph's field of view (FOV), i.e., we use it for both the in situ and HI observations.

Especially useful is the following concept based on earlier work by Sheeley et al. (1999) and demonstrated with *STEREO*/HI and SMEI by, e.g., Rouillard et al. (2008, 2009), Davis et al. (2009), Möstl et al. (2009b, 2010), and Howard & Tappin (2009b): if an ICME propagates with constant velocity and direction to large angles with respect to the Sun, an observer perceives deceptive angular accelerations/decelerations depending on its propagation direction relative to the observer. This effect can be used to assess the direction, velocity, and arrival time of an ICME by fitting known theoretical profiles to real-time (Davis et al. 2011) or level 2 HI or SMEI data of the ICME's elongation. There exist two practical realizations of this concept: the original technique (Rouillard et al. 2008), which assumes a point-like or negligibly narrow shape of the CME front (also called the fixed-Φ approximation; we call this fixed-Φ fitting or FPF), and the method by Lugaz (2010), which assumes a circular CME front, attached to the Sun at all times at one end (harmonic mean fitting or HMF). Note that there also exist more complex approaches to the same problem, such as the Tappin–Howard (T-H) model (Howard & Tappin 2009a, 2009b; Tappin & Howard 2009), in which a large set of pre-existing solutions is fitted to the observations, which is also useful for

real-time application, and the white-light rendering method by Wood & Howard (2009). In this study we use the FPF and HMF methods, and we present the formulae for converting elongation to distance with FP/HM and the inverted method useful for predicting ICME parameters with FPF/HMF.

The primary advantage of the fitting techniques is that they are simple and quick to apply in real time, and they can be used for single spacecraft HI observations, which will most likely be available on future solar missions or an observatory at the L5 point in the Sun–Earth system, 60° behind the Earth (Schmidt & Bothmer 1996; Gopalswamy et al. 2011). The major disadvantage is that these methods assume constant speed V and direction ϕ. In general, fast and more geoeffective ICMEs are expected to decelerate because the solar wind into which they run is usually slower and exerts a drag force, and ICME directions can be influenced by high-speed solar wind streams (e.g., Gopalswamy et al. 2009). Thus, for a real-time application, the resulting speeds and directions will only be averages of the part in which the elongation profiles are measured, and their errors have to be carefully assessed. Using two HI observatories, the assumptions of constant velocity and direction can be dropped (Liu et al. 2010a, 2010b; Lugaz et al. 2010), and again there exist two limiting cases for the "extreme" geometric assumptions of a point or a circle: triangulation (TR; Liu et al. 2010a) and tangent-to-a-sphere (TAS; Lugaz et al. 2010). An excellent summary of these techniques is given by Liu et al. (2010b).

However, what has been missing so far is a way to calculate the speeds and arrival times for the methods assuming a circular front shape (HMF and TAS). This paper aims to derive an analytical formula that gives the arrival time and velocity of an ICME using the HMF and TAS methods. The best way to independently assess the validity of any of these techniques is to check the results against in situ magnetic field and plasma measurements of ICMEs. Thus, additionally, we assess the validity of our new formula by comparing the results of the FPF and HMF methods for an ICME event on 2009 February 13–18 (see also Patsourakos & Vourlidas 2009, Kienreich et al. 2009, and Cohen et al. 2009, on the EUV wave), which we believe to be extremely well suited for this purpose for two reasons: the CME (1) had a practically constant velocity all the way in the HI FOVs, and (2) it was propagating into a "simple" slow background solar wind, so that any differences in the results by the FPF/HMF methods should be based only on the assumption of the different geometry rather than on other effects.

This paper is structured as follows. In Section 2, we present an alternative version of the Lugaz (2010) formula for inverting the harmonic mean approximation for the global ICME leading-edge shape, derived in Appendix A. An associated correction formula for calculating the arrival time using HMF is discussed in Section 2 and derived in Appendix B. In Section 3, we discuss *STEREO-A*/HI observations of the 2009 February 13–18 ICME event and application of the HMF and FPF methods. We check these results against the ICME in situ observations by *STEREO-B* and *Venus Express* (*VEX*) in Section 4. We summarize our results and present our conclusion in Section 5.

2. METHODS FOR FITTING THE TIME-ELONGATION PROFILES OF ICMEs

2.1. Fixed-Φ and Harmonic Mean

For completeness, we revisit methods for calculating a constant ICME direction and velocity from the observed elongation

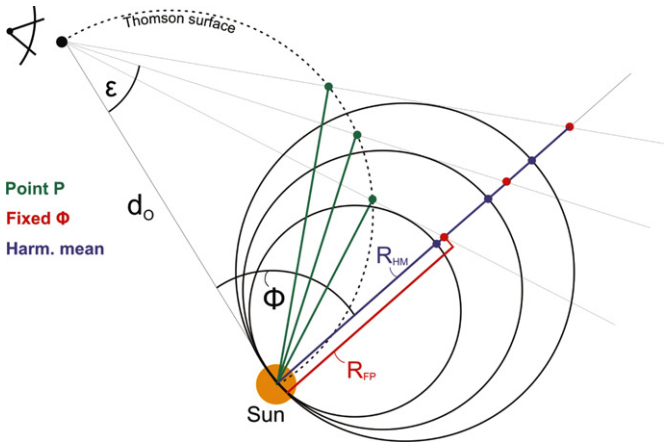

Figure 1. Illustration of the different elongation-to-distance conversion methods. From the top left, an observer looks toward a circular ICME front. The green (PP), red (FP), and blue (HM) dots show where the observer would calculate the radial distance of the ICME from the Sun using the indicated methods. In this case, the observer used the same direction ϕ for the FP and HM conversion equations, which leads to $R_{\rm FP} > R_{\rm HM}$ for the same elongation value.

(A color version of this figure is available in the online journal.)

variation with time $\epsilon(t)$ of a feature (often the ICME leading edge) in the HI FOVs. For two excellent in-depth summaries, see Lugaz (2010) and Liu et al. (2010b). We will restrict ourselves here to a short discussion and introduce definitions to be used in this case study. We present in this section (1) a new alternative version of a formula that can be used to fit time-elongation tracks of transients assuming a circular front shape (harmonic mean fitting or HMF; Lugaz 2010), and (2) a new geometrically consistent formula for deriving the ICME arrival time at a given location in the heliosphere with HMF. The formulae are derived in Appendices A and B.

The effects of observing features of ICMEs at large angles to the Sun were introduced by Sheeley et al. (1999). Basically, the assumption that the CMEs intensity signal originates from the plane of sky (POS), as valid in the coronagraph FOVs close to the Sun, is not valid for larger angles from the Sun (Vourlidas & Howard 2006; Howard & Tappin 2009a). The radial distance $R_{\rm FP}$ from the Sun of a point-like transient moving at a longitude ϕ ($\phi > 0$ is defined as westward) relative to the observer, who is situated at a distance d_o from the Sun, which is observed at time t at an elongation angle ϵ, is given by Sheeley et al. (1999, their Equation (B1)) as

$$R_{\rm FP}(t) = \frac{d_o \sin\epsilon(t)}{\sin(\epsilon(t)+\phi)}. \quad (1)$$

This is also known as the fixed-ϕ (FP) approximation (Kahler & Webb 2007). These definitions are visualized in Figure 1. Solving for $\epsilon(t)$ leads to

$$\epsilon(t) = \arctan\left(\frac{V_{\rm FP} t \sin(\phi_{\rm FP})}{d - V_{\rm FP} t \cos(\phi_{\rm FP})}\right), \quad (2)$$

first written explicitly by Rouillard et al. (2008). Here we have already replaced the distance $R_{\rm FP}$ with $V_{\rm FP}t$. This formula is thus based only on a constant velocity $V_{\rm FP}$ and a constant direction $\phi_{\rm FP}$. For comparison with real data, it is also necessary to obtain a launch time $t_{0\rm FP}$ on the Sun, for which $\epsilon(t_{0\rm FP}) = 0$.[7] Equation (2)

[7] We note that for a consistent comparison of the launch time to solar surface signatures, any $\epsilon(t_0)$ should be set to the angular size of the Sun's radius (≈0.°26 for an observer at 1 AU), but to simplify the arrival time calculation $\epsilon(t_0) = 0$ in this paper.

has the obvious advantage that a theoretical elongation profile can be fitted in a least-squares sense to the observed values of $\epsilon(t)$, which results in the three parameters $V_{\rm FP}$, $\phi_{\rm FP}$, and $t_{0\rm FP}$ (e.g., Rouillard et al. 2008, 2009; Davis et al. 2009, 2010; Möstl et al. 2009b, 2010; Lugaz 2010). We further call this the fixed-ϕ-fitting or FPF approach. We implemented the fitting by using a downhill simplex method (Nelder & Mead (1965), IDL function `amoeba.pro`) which is, from our experience, robust for this three-parameter minimization. It can also be done by creating an "error map" for $V_{\rm FP}$ and $\phi_{\rm FP}$ and looking for the minimum residual between the theoretical and observed ICME tracks (Williams et al. 2009; Lugaz 2010).

The same procedure can be applied using the so-called harmonic mean approach. Lugaz et al. (2009) derived to convert elongation to distance a formula similar to Equation (2), but under a different assumption that the CME front can be approximated by a circle that is attached to the Sun at all times at one end. This definition is visualized in Figure 1. It is further assumed that the observer always measures the resulting elongation angle by looking along the tangent to this circle (see Figure 1 and Lugaz et al. 2009; Howard & Tappin 2009a). The radial distance of the circle's apex $R_{\rm HM}$, the point with the greatest distance from the Sun, is given by Lugaz et al. (2009):

$$R_{\rm HM}(t) = \frac{2d_o \sin\epsilon(t)}{1+\sin(\epsilon(t)+\phi)}. \quad (3)$$

An equivalent formula was also derived by Howard & Tappin (2009a, their Equation (41)). We derived a new version of the inversion of this formula in Appendix A, compared to the one given by Lugaz (2010). Setting $R_{\rm HM} = V_{\rm HM}t$ and defining

$$a = \frac{2d_o}{V_{\rm HM}t} - \cos\phi_{\rm HM}, \quad b = \sin(\phi_{\rm HM}), \quad (4)$$

leads to

$$\epsilon(t) = \arccos\left(\frac{-b + a\sqrt{a^2+b^2-1}}{a^2+b^2}\right). \quad (5)$$

This has only one term, in contrast to the formula with two terms given by Lugaz (2010). The reason we use this formula instead of Equation (1) from Lugaz (2010) is that we found it works more robustly when running the downhill simplex method for the fitting, which we use in contrast to Lugaz (2010), who constructed error maps for a grid of $V_{\rm HM}$ and $\phi_{\rm HM}$ values. Our purpose is to find out if the two approaches can produce different results in future studies and to further check the robustness of our fitting method, but in this paper we restrict ourselves to discussing the results of the simplex method alone.

2.2. Arrival Time Calculation Using Fitting Methods

In this section, we summarize the calculation of the arrival time t_a of an ICME at a particular planet or spacecraft for both fitting methods. In addition to the constant direction, the FPF and HMF methods result in a constant velocity $V_{\rm FP}/V_{\rm HM}$ and a launch time $t_{0\rm FP}/t_{0\rm HM}$ on the solar surface, for which $\epsilon(t_0) = 0$. For the FPF method, the arrival time is then given simply by

$$t_{\rm aFP} = t_{0\rm FP} + d_i/V_{\rm FP}, \quad (6)$$

with d_i being the radial distance of the in situ observing spacecraft from the Sun. For the FPF method, it is assumed that the ICME's white-light emission arises from a single plasma element, or in reality that the ICME front is of negligible small extent along the line of sight. However, what does a "small extent" mean, exactly? In this respect, it is necessary to define in which cases an ICME with a direction $\phi_{\rm FP}$ is actually expected to hit a spacecraft. It has been assumed in previous studies (e.g., Davis et al. 2009, 2010) that if the direction $\phi_{\rm FP}$ matches the in situ spacecraft longitude to within a few degrees, the ICME is expected to hit the spacecraft, and the arrival time can be calculated by using Equation (6). This actually implies that the front shape of the ICME for the FPF method is a small segment (extending a few degrees in longitude) of a circle with a radial distance of 1 AU from the Sun around the direction $\phi_{\rm FP}$. However, for larger angular separations between the in situ spacecraft and the ICME direction, this definition runs into trouble because it is unclear if the ICME is expected to hit the spacecraft at all. Clearly, only a statistical study using many ICMEs will determine where to set the boundary at which a prediction should be issued that an ICME will hit a particular planet or spacecraft at a certain longitudinal separation angle (which we further call Δ) between the ICME direction and the target position.

This problem is less evident for the HMF method because the ICME front shape is well defined as an expanding circle attached to the Sun at one end. However, the opposite problem arises here compared to the FPF method: there it is not clear if a spacecraft is hit at all by an ICME, but here sooner or later *every* in situ spacecraft should detect the ICME front, which is positioned at a longitude of $\phi_{\rm HM} \pm 90^\circ$, i.e., in the half-space centered on $\phi_{\rm HM}$. Nevertheless, the well-defined circular geometry directly leads to an analytical arrival time calculation, which we derive in Appendix B. To calculate an ICME arrival time at a given heliospheric position that is geometrically consistent with the circular front, it is necessary to correct for the fact that all parts of the circular front except the apex will always arrive later than the apex at a given radial distance from the Sun (see also Figure 8(a)). To calculate the arrival time of an ICME at a given heliospheric distance d_i and at a longitudinal separation Δ with the HMF method, an arrival time correction t_c must be added to the arrival time of the ICME apex:

$$t_{\rm aHM} = t_{0\rm HM} + \frac{d_i}{V_{\rm HM}} + t_c. \quad (7)$$

As derived in Appendix B, this can be reduced to the simple equation

$$t_{\rm aHM} = t_{0\rm HM} + \frac{d_i}{V_{\rm HM}\cos(\Delta)}. \quad (8)$$

It is clearly seen that the circular HM geometry leads to the elementary result that the speed of the ICME flank at a given angle Δ to the ICME apex is only reduced by a factor $\cos(\Delta)$, for this particular geometry. This is especially important for comparison to in situ measurements of the solar wind bulk speed when using the HMF method, where the speed $V_{\rm HMI} = V_{\rm HM}\cos(\Delta)$ has to be used, in contrast to FPF, where only $V_{\rm FP}$ has to be taken.

In addition, there exists a triangulation version of the HMF approach, which was called the TAS method (Model 1 in Lugaz et al. 2010). In contrast to the single-spacecraft fitting methods, using two $\epsilon(t)$ functions gained by widely separated observers makes it possible to relax the assumptions of constant speed V and direction ϕ (see also Liu et al. 2010a, 2010b). To calculate the ICME arrival time with TAS, Equation (8) also has to be

used, but because $V_{\rm TAS}(t)$ and $\phi_{\rm TAS}(t)$ are now functions of time, a final speed and final direction have to be put into Equation (8), i.e., the resulting speed and direction values at the last timestep, both $\epsilon(t)$ functions, could be determined. Note that the final direction $\phi_{\rm TAS}$ is simply the result of the last $\epsilon(t)$ pair, but for the terminal propagation speed $V_{\rm TAS}$ averages of the last few hours need to be taken because of the fluctuations resulting from the derivatives (see e.g., Figure 4 in Liu et al. 2010a). Alternatively, the arrival time correction t_c, which is given by Equation (B5) in easy-to-use units, needs to be added to an already calculated arrival time of the ICME apex at a given radial distance from the Sun.

Before proceeding to a data example, we also note that we extract the ICME track from *STEREO-A*/HI images in the same plane (the ecliptic) where the main in situ observing spacecraft (*STEREO-B*) is situated. In this way, we avoid any effects based on observations and positions yielding from different latitudes.

3. CASE STUDY OF THE 2009 FEBRUARY 13–18 ICME

On 2009 February 13, a CME erupted from a small bipolar active region (AR 11012) at position S04E46 as seen from Earth (Kienreich et al. 2009; Miklenic et al. 2011). It was associated with a *GOES* class B2.3 flare peaking at 05:46 UT and an EUV wave, the latter being discussed by Kienreich et al. (2009), Patsourakos & Vourlidas (2009), and Cohen et al. (2009). Between 2009 February 13 and 18, *STEREO-B* was situated on average at 1.0033 AU and at a longitude of $-47\overset{\circ}{.}6$ east of the Earth in Heliocentric Earth Ecliptic (HEE) coordinates, *STEREO-A* at $43\overset{\circ}{.}5$ west of the Earth at 0.9643 AU, and their separation in the HEE latitude was negligible ($<0\overset{\circ}{.}3$). This means that the event was seen at the limb from *STEREO-A* and almost exactly at disk center by *STEREO-B*, making this a practically perfect quadrature configuration, as the *STEREO* longitudinal separation was 91°. The two probes are equipped with instruments (*SECCHI*; Howard et al. 2008) to image the Sun's corona in the extreme ultraviolet spectrum (EUVI), and the inner (COR1, 1.5–4 $R_\odot$) and outer coronae (COR2, 2.5–15 $R_\odot$) in white light. Images of the heliosphere, also in white light, are obtained by the HIs (*SECCHI*/HI; Eyles et al. 2009), with HI1 covering 4°–24° elongation from the Sun and HI2 $18\overset{\circ}{.}7$–$88\overset{\circ}{.}7$. These values are valid for the ecliptic plane, at which the optical axes of the HI telescopes are pointing nominally. *STEREO* is also able to probe the solar wind at the position of each spacecraft itself with two in situ instruments: *IMPACT* (Luhmann et al. 2008) and *PLASTIC* (Galvin et al. 2008).

Miklenic et al. (2011) discussed the early acceleration phase of the event and found that the CME reached its propagation velocity of 350 km s^{-1} at around 2.5 $R_\odot$, which is still in the FOV of the *STEREO*/COR1A coronagraph and thus is rather close to the Sun and well below the HI FOVs. The ICME was detected in situ by the *STEREO-B* and *VEX* (see Section 3.2), with an observed average proton bulk speed at *STEREO-B* also of ≈350 km s^{-1}. The state of the background solar wind for this event is discussed by Temmer et al. (2011) using the WSA/MAS+ENLIL solar wind model (Odstrcil 2003). They found a rather simple state of the heliosphere around the time and location of the eruption, with a small high-speed stream to the east of the source region. *STEREO-B* EUVI images also show that the AR 11012 was the only one on the solar disk viewed from the location of *STEREO-B*.

In summary, the CME was slow, reached its terminal velocity very close to the Sun, and propagated into a simple, slow solar wind, approximately maintaining its constant velocity from 2.5 $R_\odot$ up to 1 AU (215 $R_\odot$; see also Rollett et al. 2011). These characteristics make the event especially well suited for a comparison between the HMF and FPF methods, because the ICMEs propagation in the HI FOVs, where the methods are applied, will not be strongly affected by any interaction with fast streams from coronal holes (e.g., Gopalswamy et al. 2009) or other ICMEs, thus minimizing the effects of a possible deflection or acceleration during its propagation through the *STEREO-A* FOVs, which would be in conflict with the FPF/HMF assumptions of constant velocity and constant direction. Thus, any differences in the results may be safely ascribed to the strongly different assumptions of the shape of the ICME front as used for FPF/HMF.

3.1. STEREO-A Heliospheric Imaging Observations

In Figure 2, the top two images show running differences of the ICMEs evolution in *STEREO*–HI1A, and the bottom two images show HI2A. The intensities in the images are related to Thomson scattering of white-light solar radiation off solar wind electrons, and the incident intensity for a given observer maximizes along the line of sight at the Thomson surface (Vourlidas & Howard 2006; Howard & Tappin 2009a; see also Figure 6). The reader is referred to the HI1A/HI2A movie in the online journal. Overall, the CME is rather small and faint. It is actually so faint that it cannot be discerned in *STEREO-B* HI movies; thus, the observations limit our study to using single-spacecraft HI methods and it is not possible to use any triangulation approaches. As seen in the first image, the ICME clearly has a ring-like shape with a small angular width of roughly 20°, which is consistent with a view of a croissant-shaped ICME edge-on (Thernisien et al. 2009; Wood & Howard 2009), i.e., we look along the axis of the ICME, which is pointing out of the paper plane. The second density enhancement at its sunward end disappears around −15° elongation, leaving only the leading edge visible.

We estimated the ICMEs angular width (AW) in HI using the method from Lynch et al. (2010, results denoted by $\rm AW_L$) and additionally by a direct measurement in the POS of *STEREO-A* (denoted by $\rm AW_D$). The results are indicated in Figure 2 for each frame and show that between early February 14 and late February 15, AW remained between 19° and 27°, which is practically constant. In the online movie, it is also seen that neither the angular width nor the latitudinal propagation direction and the morphology significantly change during the full propagation in the HI FOVs. Later than early February 16, the ICME becomes very faint in a running difference image, but its leading edge can still be seen in the Jmap (see below and Figure 3(b)).

In the right two images of Figure 2 it is also seen that the ICME propagates along a central position angle (P.A.) about 2° north of the ecliptic plane, and the latter is drawn at a P.A. of $92\overset{\circ}{.}0$ in the *STEREO-A* POS. The ICMEs central P.A. in the HI1 frame is $87\overset{\circ}{.}5$, and $90\overset{\circ}{.}5$ in the HI2 frame. Thus, in latitude, the ICME propagates outward close to the ecliptic, and thus close to *STEREO-B* (at P.A. = $92\overset{\circ}{.}0$) and *VEX* (at P.A. = $90\overset{\circ}{.}3$). The heliospheric longitude of *STEREO-B* is only 1° east of the Solar source region of the CME, and *VEX* is located 21° to the west of it, at a radial distance of 0.7185 AU and an HEE longitude of $-25\overset{\circ}{.}4$ (roughly halfway between *STEREO-B* and the Earth). Thus, judging from the location of the Solar source region, the spacecraft positions and the symmetry axis close to the ecliptic plane the ICME are expected to hit both *STEREO-B* and *VEX*.

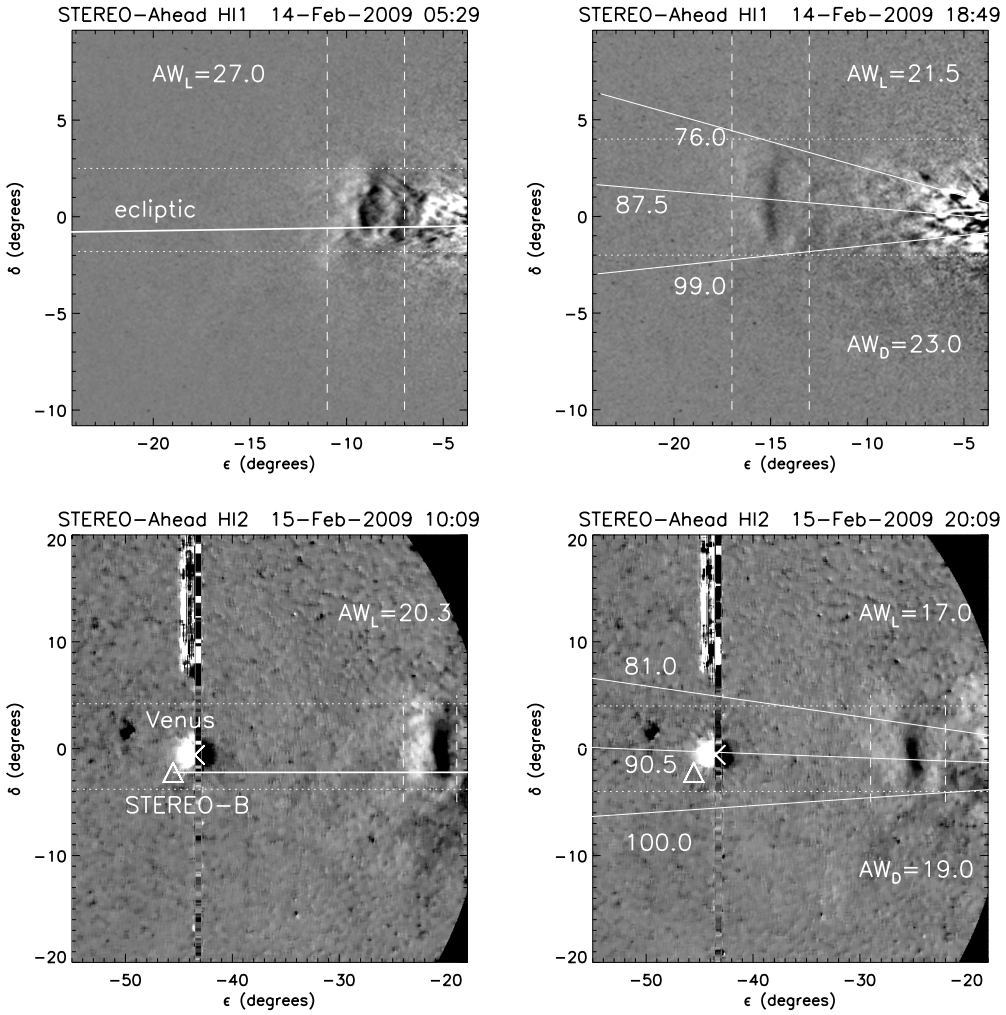

Figure 2. Evolution of the ICME in *STEREO-A* HI1 (top two images) and HI2 (bottom two images). The ICME is delimited in elongation ϵ and elevation δ by dashed and dotted lines, respectively. These coordinates represent longitude (ϵ) and latitude (δ) in a Helioprojective Cartesian (HPC) coordinate system. In the left two images, the ecliptic (in the plane of sky of *STEREO-A*) is plotted by a dash-dotted line. The positions of *STEREO-B* (triangle) and *VEX* (cross) are indicated in the bottom images. In the right two images the upper, central, and lower position angles of the ICME are indicated, again for the plane of sky of *STEREO-A*, giving a directly measured angular width of $\mathrm{AW}_D = 23^\circ$ (HI1) and $\mathrm{AW}_D = 19^\circ$ (HI2). The angular widths AW_L in all images are based on the formula by Lynch et al. (2010), and are quite similar to the AW_D values. The small angular width and the morphology are consistent with a CME viewed edge-on, so its axis of symmetry points out of the paper plane.

(An animation of this figure is available in the online journal.)

Figure 3(a) shows the proton density N_p observed by *STEREO-B*. Figure 3(b) shows a Jmap extracted along the ecliptic plane. This is done by vertically stacking the median of the central rows ±16 pixels in the *STEREO-A* HI1/2 running difference images (for further details, see Davies et al. 2009). It is seen that early on 2009 February 18, a rise in N_p corresponds to the arrival of a track in the Jmap, which is the leading edge of the ICME seen in Figure 2. The track in the Jmap was manually selected by choosing 30 points along the front of the leading edge. This procedure was repeated 10 times. From the uncertainties associated with the manual selection of the points, we will discuss how the results of the fitting procedures are affected, so all systematic errors are assumed to arise from the manual selection only. The measured points were then interpolated onto an equidistant temporal grid also consisting of 30 points (see Figure 3(c)).

3.1.1. Results of the Fitting Methods

We now apply the FPF and HMF methods, as introduced in Section 2, to the measured ICME track. Figure 3(c) shows the results, where the fitting functions (red: FPF; blue: HMF) are shown along with the observed $\epsilon(t)$ and the error bars arising from the manual selection of the track. Both methods reproduce $\epsilon(t)$ very well, but the results for the free parameters differ considerably (see also Table 1):

$$\phi_{\mathrm{FP}} = -79^\circ, \quad V_{\mathrm{FP}} = 280\ \mathrm{km\ s^{-1}}, \tag{9}$$

$$\phi_{\mathrm{HM}} = -107^\circ, \quad V_{\mathrm{HM}} = 322\ \mathrm{km\ s^{-1}}, \tag{10}$$

so the HMF direction is 28° eastward (or further away from the observer) compared to FPF. This has been noted by Lugaz (2010) to be a general feature—especially for a limb event the observer will mostly see the flank of the ICME in HI because of the scattering at the Thomson surface. By "flank" we denote those parts of the ICME front that are closer to the Sun compared to the apex, the point along the circle with the greatest distance from the Sun. The HMF method corrects this effect and will put the ICME apex direction always farther away from the observer compared to FPF (Lugaz 2010). In this case, the direction for FPF is 12° west of the longitude of *STEREO-B* and for HMF 16° east.

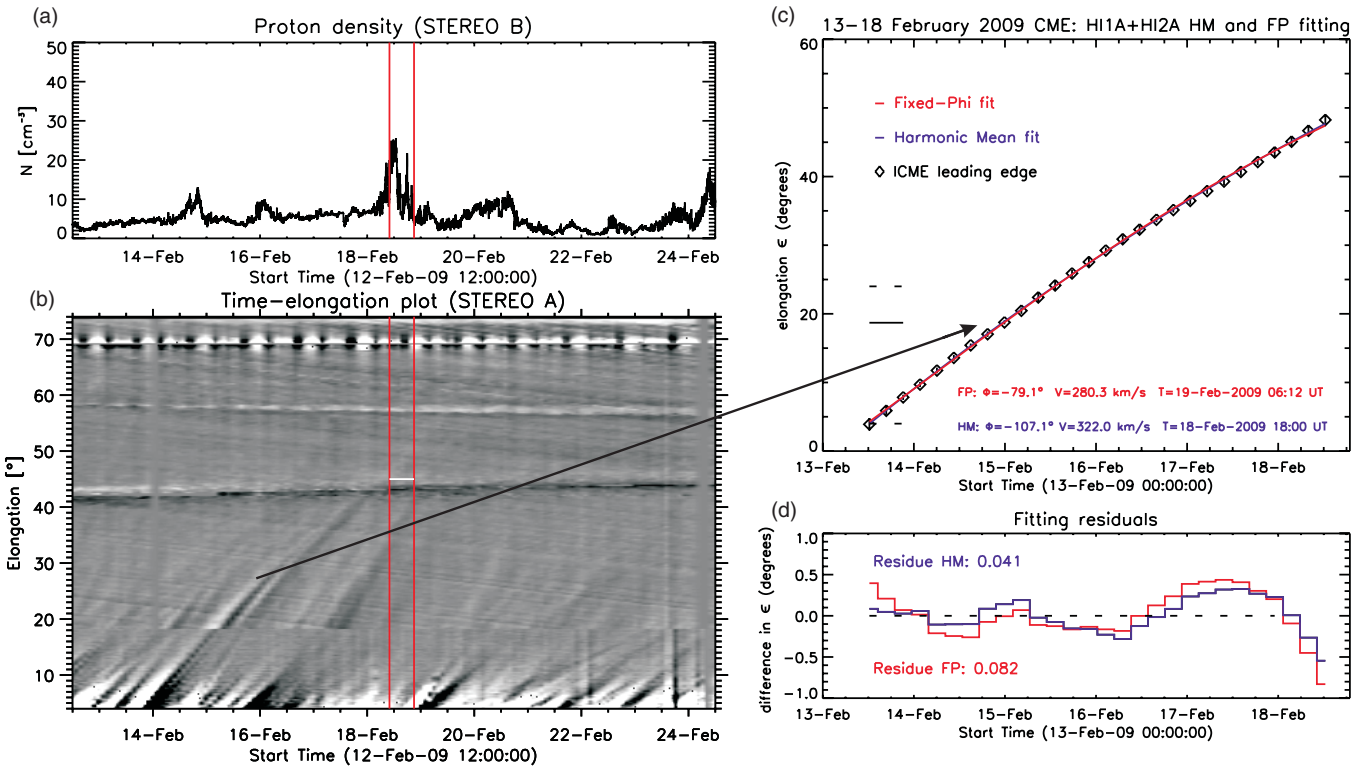

Figure 3. (a) Proton density observed by *STEREO-B/PLASTIC*. Enhanced densities (up to 25 protons cm^{-3}) in front of the flux rope are delimited by two vertical lines, with the left one setting the arrival time. (b) Jmap along the ecliptic plane with the elongation of *STEREO-B* marked by a white horizontal line. It is seen that a track, starting on February 13, reaches the elongation of *STEREO-B* and *VEX* early on February 18, which matches very well the single density jump observed by *STEREO-B*. (c) Best HMF/FPF fits for the ICME leading edge. Both functions are able to reproduce the observed function $\epsilon(t)$. (d) Residuals between the fitting functions and the observations. The time development of $\epsilon(t_i) - \epsilon_{\rm fit}(t_i)$ is similar for both techniques, and the summarized residue σ^2 for HMF is half the value for FPF.

(A color version of this figure is available in the online journal.)

Table 1
Compilation of Observed Parameters and Results of Fitting Techniques for the 2009 February 13–18 ICME

Technique	Instruments	$R_\odot$	l (deg)	V (km s^{-1})	t_0, UT	t_a, UT
Flare peak	*GOES*	1	−89.5	···	Feb 13 05:46	···
tracking	COR1A	2.5	−91[a]	350[a]	Feb 13 06:20	Feb 18 03:57[b]
FPF/B	HI1/2A	14.1–203.7	−79	280	Feb 13 01:30	Feb 19 06:12
HMF/B	HI1/2A	14.7–225.7	−107	322/310[c]	Feb 13 03:20	Feb 18 18:00
STB	*IMPACT/PLASTIC*	215.6	−91	362/348[d]	···	Feb 18 10:00
FPF/V	HI1/2A	14.1–203.7	−79	280	Feb 13 01:30	Feb 17 12:01
HMF/V	HI1/2A	14.7–225.7	−107	322	Feb 13 03:20	Feb 18 02:36
VEX	*MAG*	154.5	−68.9	···	···	Feb 17 22:00

Notes. The results for COR1A are taken from Miklenic et al. (2011). FPF: fixed-ϕ fitting; HMF: harmonic mean fitting; the suffix "/B" indicates results for *STEREO-B*, "/V" for *VEX*. Column $R_\odot$ indicates the range of solar radii where the measurements were obtained or techniques were applied. For the fitting methods, this is the range of the distances $R_{\rm FP}$ and $R_{\rm HM}$ corresponding to the first and last $\epsilon(t)$ measurements of the ICME track in the Jmap. Angle l is the longitude of the source region (flare peak), the ICME direction (FPF/HMF), and the spacecraft positions (*STEREO-B*/*VEX*) with respect to the *STEREO-A* spacecraft ($l > 0$ for solar west). V is the CME/ICME speed, and t_0/t_a are the launch and arrival times, respectively.

[a] The COR1A speed was measured in the plane of sky by Miklenic et al. (2011).

[b] Ballistic projection of the CMEs arrival at *STEREO-B* with the COR1 measurements.

[c] The first speed is for the apex of the HM circle ($V_{\rm HM}$) and the second is for the flank part hitting *STEREO-B* ($V_{\rm HMI}$).

[d] The in situ V are means over the ICME sheath/flux rope regions.

The expected in situ speed of $V_{\rm HMI} = 310$ km s^{-1} at the location of *STEREO-B* is 30 km s^{-1} faster compared to FPF. We attribute this again to the fact that for a limb ICME event, especially one with low axis inclination to the ecliptic (to be justified further in the next section), more and more of the ICME flank is sampled. For a circular front, points at the flank will always move more slowly than the ICME apex, and again the HMF technique corrects this effect, which results in a higher speed compared to FPF (Lugaz et al. 2011). Because the launch times t_0 are quite similar (see Table 1 for a summary), the different speeds lead to quite different arrival times. Due to its higher speed, $t_{\rm aHM}$, which already includes the arrival time

correction presented in Section 2, is about 12 hr earlier compared to FPF, which is a considerable difference.

In Figure 3(d), we demonstrate how well both fits are able to reproduce the observed function $\epsilon(t)$. To this end, we use the fitting residual (Williams et al. 2009; Lugaz 2010)

$$\sigma^2 = 1/N \sum_{i=1}^{N} (\epsilon(t_i) - \epsilon_{\rm fit}(t_i))^2, \quad (11)$$

with N being the number of data points along the ICME track and $\epsilon_{\rm fit}$ being the calculated elongation value for the time step t_i using the given set of fitting results V, ϕ, and t_0. For the least-squares minimization using the downhill simplex method, a slightly modified σ^2 is used, where we replace both ϵ terms with their norms $|\epsilon(t_i)|$ and $|\epsilon_{\rm fit}(t_i)|$, leading to a more robust minimization than Equation (11). From Figure 3(d), where we plotted $\epsilon(t_i) - \epsilon_{\rm fit}(t_i)$ for every $\epsilon(t)$ measurement, it is seen that both functions are able to describe almost equally well the observed elongation variation of the ICME leading edge. The residual σ^2 is a factor of two higher for FPF than for HMF, and both residual functions follow each other very closely, with the strongest deviations from the observed elongations at the end of the track. Nevertheless, based on the fits, one cannot clearly distinguish between the two methods considering that a goodness of fit is better for one method as compared to the other. A real-time space weather predictor would thus not be able to distinguish whether one of the predictions should be preferred over the other because he/she is able to fit the $\epsilon(t)$ function with almost the same accuracy with both methods. To the contrary, both functions have three free parameters and are flexible enough to fit $\epsilon(t)$ almost perfectly, but the results of the inversion differ significantly due to the vastly different assumed geometries. Thus, the only way to distinguish between the success of the two methods is to determine whether the independent in situ observations, available for this event even by two spacecraft, are consistent with the results derived from the HIs. However, before we proceed to discussing the in situ data, we must assess the errors involved in the derived parameters.

3.1.2. Error Analysis

How do the errors arising from the manual selection of the ICME track in the Jmap impact the results of the FPF and HMF methods? To answer this question, we constructed two additional tracks

$$\epsilon_+(t) = \epsilon(t) + 2\sigma_\epsilon(t), \quad (12)$$

$$\epsilon_-(t) = \epsilon(t) - 2\sigma_\epsilon(t), \quad (13)$$

with $\sigma_\epsilon(t)$ being the standard deviation of $\epsilon(t)$. Thus, $\epsilon_+(t)/\epsilon_-(t)$ is the track with the maximum positive/negative deviation from $\epsilon(t)$. We again fitted the two tracks of maximum deviation with the FPF and HMF methods and averaged the difference between these results and the ones for $\epsilon(t)$ (Table 1) to obtain an error for V, ϕ, t_0, and t_a. For t_a, the HMF arrival time correction has to be included. We found a mean standard deviation of $2\sigma_\epsilon = 0.^\circ51$ arising from the manual selection of points; thus, the systematic error associated with the manual measurement in the Jmap is about $\pm0.^\circ5$. This error affects the direction as $\phi_{\rm FP} = -82^\circ \pm 1.^\circ8$ and $\phi_{\rm HM} = -111^\circ \pm 2.^\circ8$. The errors in the speeds are $V_{\rm FP} = 288 \pm 5.0\,{\rm km\,s^{-1}}$ and $V_{\rm HM} = 332 \pm 8.7\,{\rm km\,s^{-1}}$, again slightly higher for HMF. The errors in launch times are ±1 hr 35 minutes (FPF) and ±1 hr 27 minutes (HMF). Most importantly, the arrival time errors are ±54 minutes (FPF) and ±20 minutes (HMF), where we quoted the values for the location of *STEREO-B*. Interestingly, the error is less for the HMF method by about a factor of two, which arises from the property that the arrival time correction partly compensates for the error in the arrival time due to the slightly different ϕ. Note that the arrival time error of less than 1 hr is much shorter than the difference of 12 hr in t_a between the two methods (see Table 1). It is clear that these errors are rather small because we used a very long track that reaches completely up to the elongation of the spacecraft in the Jmap. We will test the accuracies and errors of shorter tracks in Section 3.3, but first we compare the results obtained in this section with independent multi-point in situ data.

3.2. STEREO-B, VEX, and ACE In Situ Observations

The *STEREO-B* spacecraft was situated at -91° (HEE longitude) to *STEREO-A* during our event. This is $\Delta_B = -9^\circ$ and $\Delta_B = +20^\circ$ away from the ICME directions given by FPF and HMF, respectively. Thus, the directions from both methods indicate that the ICME will hit *STEREO-B*. Figure 4 shows the proton bulk parameters (Galvin et al. 2008) and the magnetic field (Luhmann et al. 2008) measured in situ. Because of its low velocity, the ICME does not drive a clear shock, but between 2009 February 18 08:00 and 10:00 UT, two shock-like features mark the transition from a very slow solar wind (300 km s^{-1}) to an enhanced density region traveling with 350–360 km s^{-1}. We thus define the arrival time at *STEREO-B* t_B = February 18 10:00 UT, which marks the beginning of the proton density enhancement (first vertical guideline). Because we tracked the leading edge of the ICME in the Jmap, also related to the most enhanced densities, this is the time that has to be used for assessing the arrival time predictions. After what could be a small-scale flux rope, a discontinuity around February 18 17:00 UT marks the beginning of a large-scale flux rope (diameter 0.186 AU), which is not a magnetic cloud (Burlaga et al. 1981) because the magnetic field is not smooth and the temperature is higher compared to its environment. Nevertheless, visually it can be perceived that the field rotates as the B_N component (in this case the poloidal one) goes from north to south and B_T (the axial component) is negative or eastward, throughout the flux rope interval. Assuming this rotation is caused by the spacecraft going through a helical flux rope, it is a north–south–east (NES) type and of right-handed chirality according to the classification scheme for bipolar magnetic clouds by Bothmer & Schwenn (1998). We conclude that the in situ magnetic field and plasma parameters at *STEREO-B* are in rough agreement with those seen in the HI images: a slow ICME with an axis inclination θ close to the ecliptic, and hit slightly off-center because of its northward propagation direction.

In Figure 4 we also plot the arrival times of the HMF method (the vertical dashed blue line) with the velocity $V_{\rm HMI}$ (the horizontal blue line); similarly, the FPF results are plotted in red. The difference between the arrival time predicted by HMF and the actual arrival time at *STEREO-B* is $t_{\rm aHM} - t_B = +8$ hr; positive values indicate arrival times later than predicted. For FPF, $t_{\rm aFP} - t_B = +20$ hr, so the predicted arrival is almost a day later than the observed one. Here, the new HMF method, including the arrival time correction, would have given a much better prediction. The difference in the actual arrival time is also well outside the error bars that arise from the manual selection of the ICME front. We thus attribute the residual discrepancy

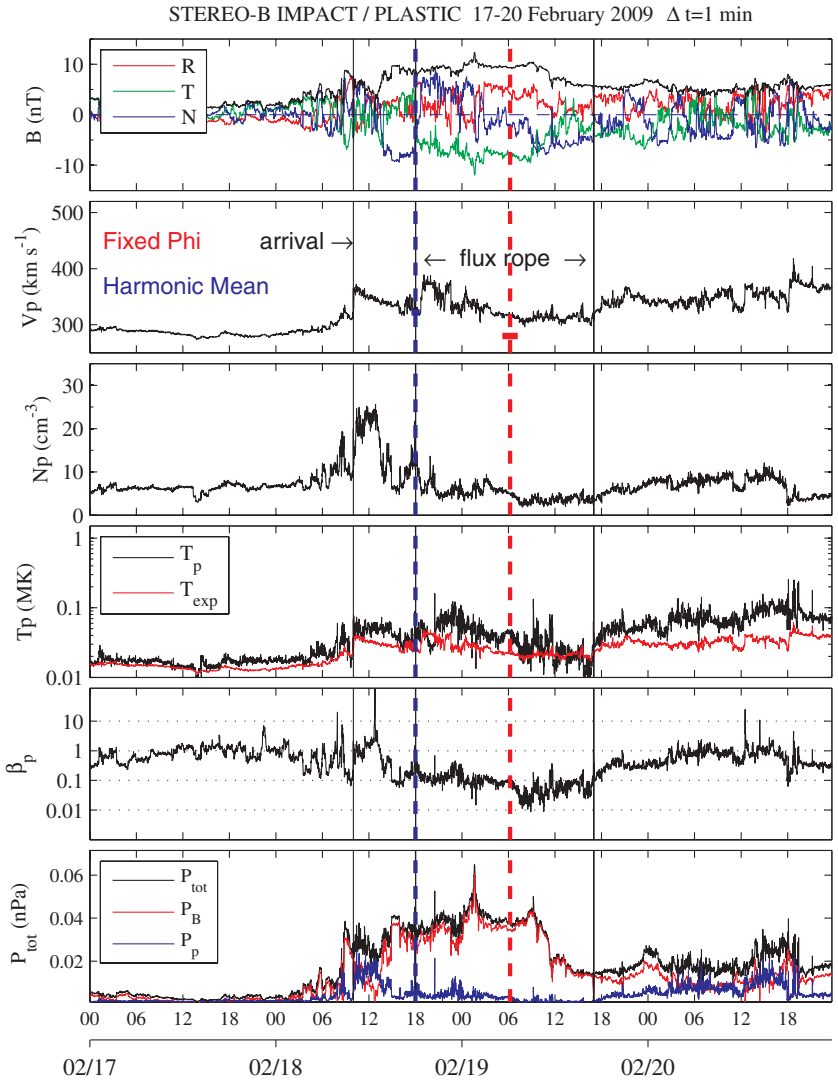

Figure 4. Magnetic field and plasma data for *STEREO-B*. The first solid line marks the approximate arrival time of the density front. The second and third solid lines indicate the flux rope interval. The arrival times from the FPF and HMF methods are given by red and blue vertical dashed lines, respectively, and the fit velocities $V_{\rm FP}$ and $V_{\rm HMI}$ are given by red and blue horizontal lines, which indicate the extent of the arrival time error ±54 minutes (FPF) and ±20 minutes, which are derived from the complete ICME track. From top to bottom: magnetic field magnitude and components in *RTN* coordinates (*R* points radially away from the Sun, *T* is the cross product of the solar rotation axis and *R*, and *N* completes the right-handed triad), proton bulk velocity, proton number density, proton temperature (black) and expected temperature (red), proton β and the total, magnetic and plasma pressure.

(A color version of this figure is available in the online journal.)

mainly to the ICME leading-edge geometry, which could clearly be different from the harmonic mean circle and associated line-of-sight effects. Nevertheless, note that the new HMF method is more accurate by about 12 hr for this particular ICME than for the original FPF method.

VEX was positioned −69° away from *STEREO-A* in longitude, so $\Delta_V = +13°$ and $\Delta_V = +42°$ away from the ICME directions given by FPF and HMF, respectively. While one will expect the ICME to hit *VEX* from the FPF method, with a direction between *STEREO-B* and *VEX*, it is not immediately clear if the HMF direction indicates a hit, though, as already previously discussed, the HMF geometry, if taken literally, will predict a hit at any spacecraft in the half-space centered on $\phi_{\rm HM}$. The arrival time correction for *VEX* is already about 30 hr at this longitudinal separation. In Figure 5, we show **B** measured by *VEX* in *Venus* solar orbital coordinates (Zhang et al. 2006), but rotated by 180° ($B_x = -B_{\rm xVSO}$; $B_y = -B_{\rm yVSO}$) so it approximately matches the *RTN* coordinates orientation we used for *STEREO-B*. We linearly interpolated over time intervals when *VEX* was below three *Venus* radii to see only the solar wind magnetic field. A magnetic flux rope interval, with a smooth rotation during an elevated field strength of about 10 nT, is found to start at 2009 February 17 22:00 UT, which we define as the *Venus* arrival time t_V. The interval continues until about 2009 February 18 14:00 UT. Qualitatively, its field is oriented mostly southward and westward, but it is not clearly rotating and also is not consistent with the field rotation at *STEREO-B*. However, it is very unlikely that this is connected to a different ICME event, because the ICME is seen passing over the location of *Venus*, which is very close to the location of *STEREO-B* along the line of sight in the online movie around February 18. Also, in latitude, the ICME is expected to hit *Venus* centrally. This puzzling inconsistency in the field could point out that the part of the flux rope where the field is most strongly wound and which carries the majority of the magnetic flux and helicity away from the Sun does not extend over its full length back to the Sun, but is rather

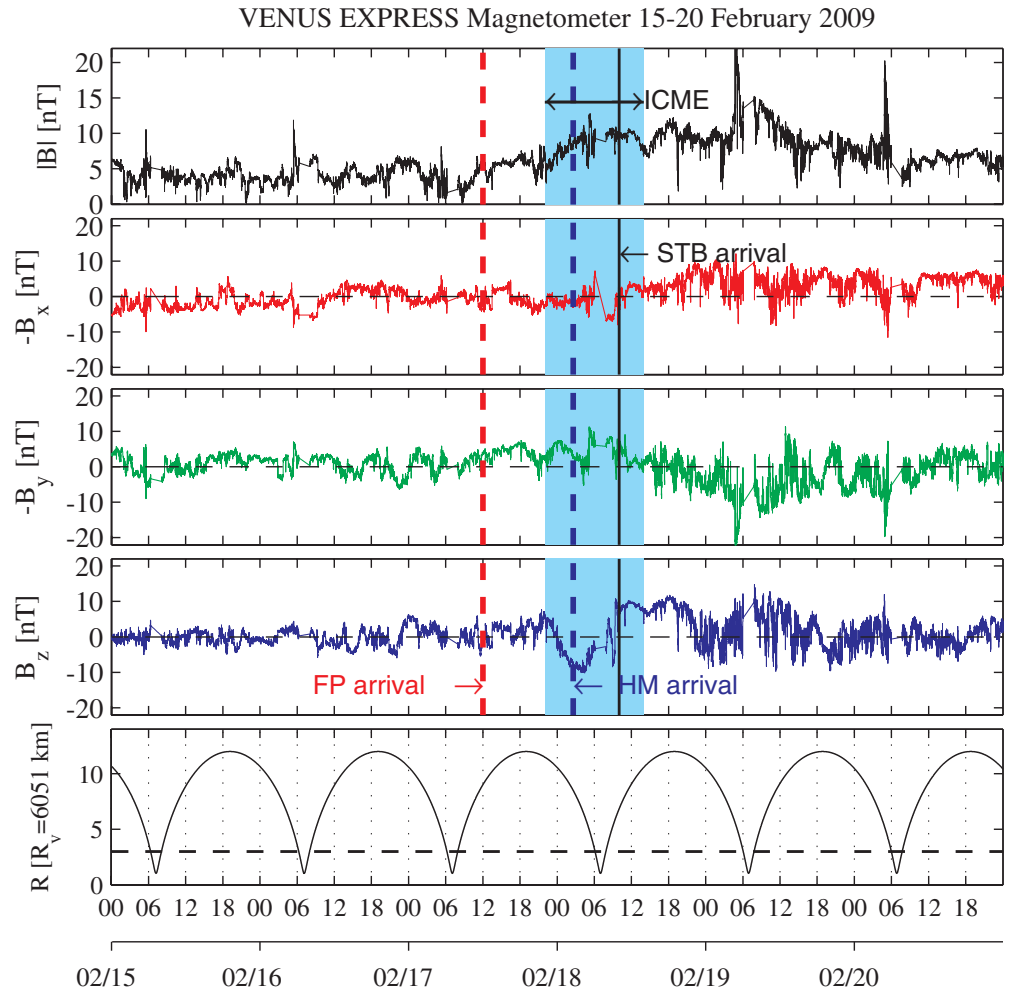

Figure 5. *Venus Express* magnetometer observations on 2009 February 15–20. Originally, the magnetic field components were given in *Venus* solar orbital coordinates, where X is directed toward the Sun, Y is opposite to the planet's orbital velocity ($\approx$ solar east), and Z points north, completing the right-handed triad. To make comparison with Figure 4 easy, we plotted here $-B_x$ and $-B_y$ components so that they approximately match the orientation of the *RTN* coordinate system (though for the position of *Venus*) used for the *STEREO-B* magnetic field components. The arrival times at *Venus* are marked again by red (FPF) and blue (HMF) dashed lines. An ICME interval of higher than average magnetic field strengths and a smoothly rotating field from February 17 22:00 UT to February 18 14:00 UT is highlighted (shaded). For comparison, the arrival time at *STEREO-B* is indicated by a solid vertical line.

(A color version of this figure is available in the online journal.)

confined around the apex of the ICME (also discussed recently by Yamamoto et al. 2010; Möstl et al. 2010; Kahler et al. 2011). The error in the arrival times for FPF was $t_{\rm aFP} - t_V \approx -10$ hr and for HMF $t_{\rm aHM} - t_V \approx +4$ hr, which means again that the consistency with the HMF method is better. However, we note that without high time resolution data for solar wind plasma parameters, it is rather difficult to set the arrival time unambiguously, and the arrival of the ICME is less well defined as for *STEREO-B*.

In Figure 6, we plot the event geometry and visualize the ICME directions and spacecraft positions. It can be seen that the circular front assumed by HMF leads to a *negative* shift in t_a compared to FPF at the position of *STEREO-B* and to a *positive* shift in t_a at the position of *VEX*, as a direct consequence of the different geometries. Both time shifts from the FPF to the HMF methods are more consistent with the in situ arrival times discussed above. The improvement in arrival time consistency is 10 hr at the position of *STEREO-B* and 4 hr at *VEX*. It is seen in Figure 6 that this arises from the circular front that touches the *STEREO-B* and *VEX* positions, despite the very different radial distances, at almost the same time (see also Figure 5).

The Earth was $-38.^{\circ}5$ and -67° away from the ICME directions given by FPF and HMF, respectively, at a heliospheric distance of 0.9877 AU. While FPF gives an arrival time of 2009 February 18 22:53 UT at the *ACE*/*Wind* satellites, a value which is quite close to the arrival time t_B at *STEREO-B* because of the almost similar heliospheric distance, the arrival time given by HMF is 7.5 days later on 2009 February 26 07:49 UT, which is due to a large arrival time correction because of the large longitudinal separation between Earth and the HM apex. We omit the plot showing the in situ data by the *ACE*/*Wind* spacecraft near Earth because there are no clear signatures of an ICME or any large-scale magnetic flux rope between February 18 and 26. This means that a longitudinal separation of 40°–70° is too far away to detect the flux rope in this case, even if it has a low axis inclination. If we assume that the ICME apex at 1 AU is close to *STEREO-B* (so the ICME travels radially outward), and the ICME has an axis inclination to the ecliptic $\theta \approx 0$, then the non-detection near Earth 47° west of the apex leads to the constraint that the longitudinal width of this slow solar-minimum ICME must be <94°, which is roughly consistent with the value of ≈70° (Wood et al.

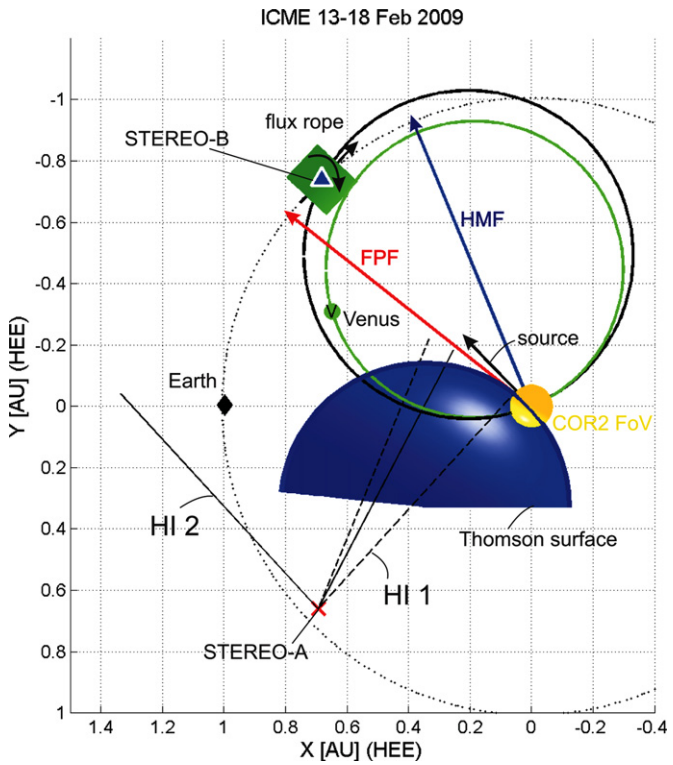

Figure 6. Illustration of the ICME directions inferred from the 2009 February 13–18 ICME event using the FPF and HMF methods, looking from north down onto the ecliptic plane. The positions of the *STEREO* spacecraft, Sun, and Earth are indicated. The black (green) circles give the shape of the harmonic mean front at the arrival time of *STEREO-B* (*VEX*). Because the HMF method assumes a circular front, the calculated arrival times at both *STEREO-B* and *VEX* match better the observed arrival times. Two black arrows show the rotation of the magnetic field inside the flux rope at *STEREO-B*; its radial size is indicated by a green cylinder.

(A color version of this figure is available in the online journal.)

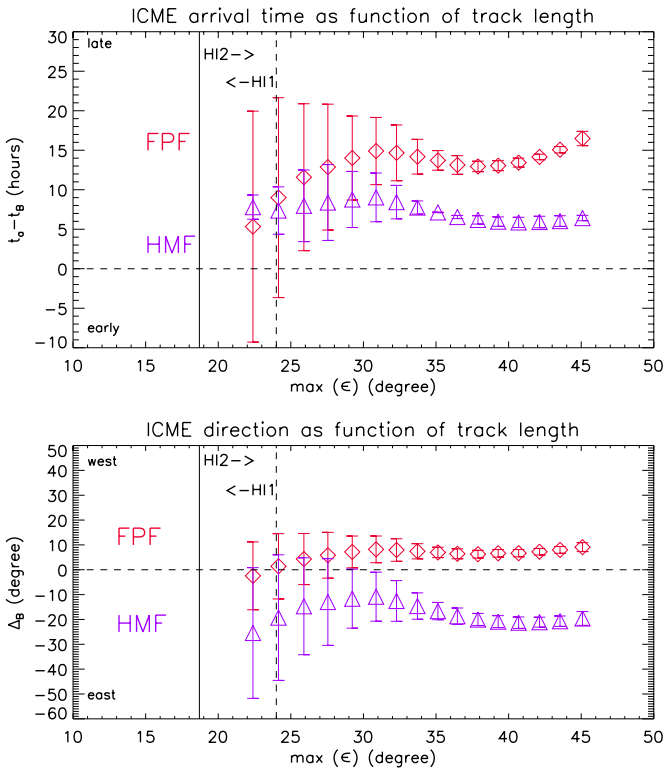

Figure 7. Accuracy of possible predictions for the ICME arrival time (upper panel) and direction (lower panel) with respect to the arrival time and location of *STEREO-B*, using different lengths for the tracks extracted from the Jmap, given by their maximum elongation value max(ϵ). Top: the difference between the arrival times t_a calculated for the FPF (red) and HMF (blue) methods and the observed arrival time t_B at *STEREO-B*. Also indicated are the outer boundary for the HI1 FOV (dashed vertical line) and the inner boundary of the HI2 FOV (solid vertical line). Bottom: differences between the calculated propagation directions ϕ and the longitude of *STEREO-B* ($\Delta_B = \phi - l_B$), as a function of max(ϵ).

(A color version of this figure is available in the online journal.)

2010) for a different slow solar-minimum ICME event observed by *STEREO*/HI, and the <60° extent obtained from multi-spacecraft in situ observations by Bothmer & Schwenn (1998).

3.3. Accuracy as a Function of Track Length

So far, we have focused on the systematic differences that arise from the different geometric assumptions underlying the two techniques. However, a major goal of future missions concerned with real-time space weather forecasting should be to have the longest possible prediction lead times. It is commonly quoted that the ICME must be observed at at least 30° from the Sun (e.g., Williams et al. 2009; Lugaz et al. 2010) to obtain reliable results with HMF and FPF. To check this statement for our case study, we plot in Figure 7(a) the error in the arrival time at *STEREO-B* as a function of the angle of the maximum ϵ measurement taken as an input for the fitting methods. We also include the error bars for t_a described in Section 3.1.2. If only the measurements from the HI1 instrument are used between $\epsilon = 4°$ and 24°, the resulting errors in the arrival time are ±12.5 hr, basically a day, for FPF, but much less for HMF, due to the compensation by the arrival time correction mentioned above. As expected, for higher values of max(ϵ) the errors, in particular for FPF, decrease and are ±4.8 hr for max(ϵ) = 30°, corresponding to a predicted lead time of about 48 hr until the actual arrival for this slow ICME. Also, for max(ϵ) > 30°, the predictions by FPF are always delayed with respect to the HMF values by ≈10 hr; thus, the systematic difference between the arrival times given by the two methods is not affected by the choice of max(ϵ).

In Figure 7(b), we plot in a similar manner the difference between the heliospheric longitude of *STEREO-B* and the propagation directions as results of the fitting methods for increasing values of max(ϵ). We do not know the exact propagation direction of the ICME, but looking at the error bars, their size clearly becomes more reasonable for max(ϵ) > 30°, where all directions range between $\Delta_B = [-20, 10]°$, and they would all have predicted a hit at the *STEREO-B* spacecraft. Also, for all times, the HMF method gives a direction further away from the observer than does FPF, and the size of the error bars evolves similarly in time.

4. DISCUSSION AND CONCLUSIONS

We discussed several new elements concerning the relationship between HIs of ICMEs obtained by *STEREO*/*HI* and their signatures observed in situ. We subjected two methods of forecasting the ICME parameters direction, speed, and arrival time to close scrutiny. These methods approximate the ICME front by a point (fixed-Φ) or a circle (harmonic mean), and the observed elongation of the ICME front as a function of time is fitted with inverted formulae to derive these parameters. We introduced (1) an alternative, simplified version of the inverted formula for the HMF method, and (2) an analytic arrival time

correction formula that is geometrically consistent with an assumed circular front shape of the ICME. It should be applied to any real-time predictions or case and statistical studies that discuss ICME arrival time calculation using methods that assume a circular ICME front, i.e., single-spacecraft HMF (Lugaz 2010) or two-spacecraft TAS (Lugaz et al. 2010).

We then checked the validity of the derived formulae by applying them in a case study to the 2009 February 13–18 ICME event, a perfect quadrature event, seen at the limb by *STEREO-A* and in situ by *STEREO-B* and *VEX*. The event was a slow event, with approximately constant speed throughout the HI FOVs. We found that the arrival time given by the HMF method was more accurate by 12 hr than the FPF method, in direct comparison to the observed in situ arrival time at *STEREO-B*. We attribute this to the fact that for an ICME with low axis inclination θ to the ecliptic, the ICME front is better described by the circular geometry assumed by harmonic mean. The low θ value was inferred independently by the morphology and small de-projected angular width of the ICME in *STEREO-A*/*HI* and the magnetic field rotation observed by *STEREO-B*. At the latter spacecraft, the rough behavior of the magnetic field components pointed to a slightly off-center hit of the ICME, consistent with a northward propagation by a few degrees of the ICME seen in HI. Thus, *STEREO-B* crossed the outer part of the cross section of the flux rope. These observations are also consistent with the view that the outer part of the flux rope is classified as an ejecta and not a magnetic cloud, with a rather flat pressure profile (Jian et al. 2006). In addition, *VEX* also observed a magnetic flux rope, about 23° west of *STEREO-B*, and again the in situ arrival time was more consistent with that predicted by HMF. We also assessed the errors in the arrival time predictions as a function of how long the ICME is visible in the heliospheric images and found that one needs to track the ICME up to 30° in elongation to obtain systematic errors (arising from the manual selection of the track only) that are less than ±5 hr when using scientific (level 2) HI data.

Our new hypothesis in this paper is that the two methods for fitting time-elongation data (HMF and FPF) simply limit cases of ICMEs with low or high axis inclination to the ecliptic, using two "extreme" assumptions of the ICME front shape (circular versus point-like). The same can also be said for the triangulation (point-like; Liu et al. 2010a) and TAS (circular; Lugaz et al. 2010) methods, which use two-spacecraft HI observations. In our hypothesis, the HMF method corresponds to the case of low axis inclination and thus a large longitudinal extent in the ecliptic (e.g., 70° for a solar-minimum low-inclination ICME; Wood et al. 2010) along the line of sight. The FPF method should give better results for an ICME with a high axis inclination, because the extent of the cross section is generally thought to be much smaller along the line of sight than its longitudinal extension (e.g., about 20° for a solar-minimum high-inclination ICME; see Kilpua et al. 2009; Möstl et al. 2009a, 2009c).

This event was especially well suited for testing this hypothesis because the assumptions of constant speed and direction of the HMF and FPF methods were approximately fulfilled; thus, the systematic differences we found should arise only from the truly different shape of the ICME front. In reality, these simplified geometric assumptions will only be rough approximations of the ICME front shape. For slow events, which tend to get swept up in corotating interaction regions and become more easily distorted, any simple geometric model might be too restrictive in general. However, for faster and more geoeffective events, where the front shape might be expected to be less easily affected by the background solar wind structure, the fitting methods could provide increasingly accurate results.

We plan to extend this type of study to a larger set of events to find out how feasible these techniques are and if they have to be extended to other geometries of the ICME front, and to further test our hypothesis concerning the differences in axis inclination. Also, one of the major questions will be if one or rather two spacecraft are necessary for an L5 or a combined L4/L5 mission (e.g., Liu et al. 2010b; Gopalswamy et al. 2011) to provide us with sufficient accuracy for advance warnings of solar eruptions using heliospheric imagers. The methods described in this paper can be used for such a mission as well as for any upcoming space weather forecasts at Earth and other planets with *STEREO*. Davis et al. (2011) showed the efficacy of using the FPF method for real-time prediction of an ICME event in 2010 April, when the *STEREO* spacecraft were separated by about 70° from Earth, which is comparable to the L5 point at 60°. There is still a long way to go, but with a solar maximum with many ICMEs before us, we will be able to extensively use *STEREO* to continue honing our skills.

C.M., M.T., and T.R. were supported by the Austrian Science Fund (FWF): P20145-N16 and V195-N16. This work has received funding from the European Union Seventh Framework Programme (FP7/2007-2013) under grant agreement 263252 (COMESEP). It is also supported by NASA grants NAS5-00132, NNG06GD41G, NNX08AD11G, NNX10AQ29G, and NNX08AQ16G. Work at the University of California, Berkeley, was supported from STEREO grant NAS5-03131. The *SECCHI* data are produced by an international consortium of the Naval Research Laboratory, Lockheed Martin Solar and Astrophysics Lab, and NASA Goddard Space Flight Center (USA), Rutherford Appleton Laboratory, and University of Birmingham (UK), Max-Planck-Institut für Sonnensystemforschung (Germany), Centre Spatiale de Liege (Belgium), Institut d'Optique Theorique et Appliquee, and Institut d'Astrophysique Spatiale (France).

APPENDIX A

ALTERNATIVE VERSION OF THE INVERTED HARMONIC MEAN FORMULA

This section explicitly shows how to solve Equation (3) for $\epsilon(t)$. This is the conversion formula from elongation to distance if one assumes that the observer looks along a tangent to a circle that is always attached to the Sun at one end ("harmonic mean" assumption, see Figures 1 and 8(a)). The radial distance of the circle's apex $R_{\rm HM}$, the point with the greatest distance from the Sun, is given by Lugaz et al. (2009):

$$R_{\rm HM}(t) = \frac{2d_o \sin\epsilon(t)}{1+\sin(\epsilon(t)+\phi)}, \tag{A1}$$

where d_o is the radial distance of the observer from the Sun, $\epsilon(t)$ is the observed elongation as a function of time, and ϕ is the constant ICME propagation direction with respect to the observer ($\phi > 0$ means solar west). After some basic algebra, Equation (A1) can be written as

$$\left(\frac{2d_o}{V_{\rm HM}t} - \cos\phi_{\rm HM}\right)\sin(\epsilon(t)) - \sin(\phi_{\rm HM})\cos(\epsilon(t)) = 1, \tag{A2}$$

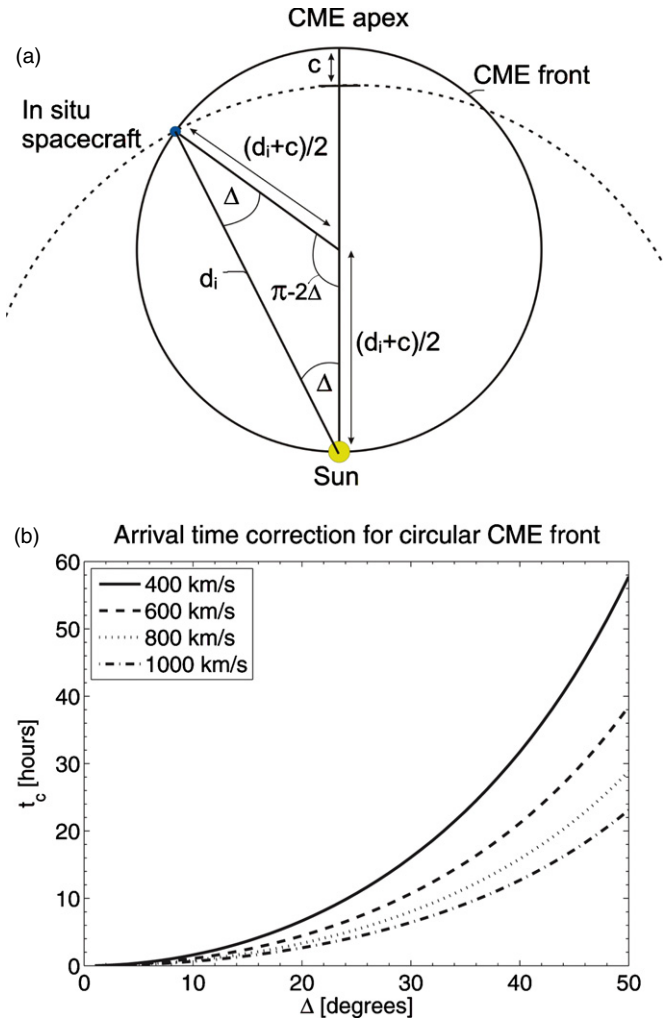

Figure 8. (a) Sketch showing the definitions and geometry for deriving the arrival time correction for the HMF and TAS methods (see the text). The solid circle is the circular front assumed for the ICME leading edge, and the dashed line depicts 1 AU. (b) The arrival time correction—Equation (B5)—is plotted as a function of the angular separation between the ICME apex and the in situ observing spacecraft I, which is situated at a radial distance of $d_i = 1$ AU from the Sun.

(A color version of this figure is available in the online journal.)

where we have already replaced distance with speed: $R_{\rm HM} = V_{\rm HM}t$. For better readability, we define

$$a = \frac{2d_o}{V_{\rm HM}t} - \cos(\phi_{\rm HM}); \quad b = \sin(\phi_{\rm HM}), \tag{A3}$$

which results in

$$a\sin(\epsilon(t)) - b\cos(\epsilon(t)) = 1. \tag{A4}$$

This equation can be brought into quadratic form by rearranging it to

$$a\sqrt{1-\cos^2(\epsilon(t))} = 1 + b\cos(\epsilon(t)) \tag{A5}$$

and squaring both sides. Solving the resulting quadratic equation in $\cos(\epsilon(t))$ leads to our form of the HMF equation:

$$\epsilon(t) = \arccos\left(\frac{-b + a\sqrt{a^2+b^2-1}}{a^2+b^2}\right). \tag{A6}$$

We conclude this section with some notes that are useful when developing a code that fits the inverse equations. While the arctan function in the FPF Equation (2) is symmetric with respect to positive and negative values of the direction ϕ, the HMF Equation (A6) will always produce positive values for $\epsilon(t)$ because of the arccos function, regardless of the sign of the direction $\phi_{\rm FP}$. Elongations provided by *STEREO-A*/HI, which looks to solar east, are negative by definition, so these $\epsilon < 0$ directly translate to $\phi_{\rm FP} < 0$ (or solar east) when applying the FPF method. For *STEREO-B*, automatically $\epsilon > 0$ and thus $\phi_{\rm FP} > 0$, consistent with our definition that $\phi_{\rm FP} > 0$ corresponds to solar west. In contrast, when applying the HMF method to *STEREO-A*, positive elongations always must be fitted, and additionally, the sign of the direction $\phi_{\rm HM}$ has to be corrected. The reason for this asymmetry is that the observer is also able to measure an ICME front with HMF even if the apex of the HM circle is on the other side of where the heliospheric imager is looking, i.e., when the apex is west of *STEREO-A* or east of *STEREO-B* (Lugaz 2010).

APPENDIX B

ARRIVAL TIME CALCULATION FOR CIRCULAR ICME FRONTS

To calculate the arrival time of a circular ICME front at a given position in the heliosphere, as assumed by the HMF (Lugaz 2010) or the TAS (Lugaz et al. 2010) methods, it is necessary to derive a formula that takes into account that different parts of the front will move with different speeds. As a consequence, the ICME arrival time will be a function not only of the radial distance of the in situ spacecraft I (or planet) from the Sun but also of its separation angle Δ to the HM apex, the point with the greatest distance from the Sun.

If the ICME in question is not heading exactly toward the in situ observing spacecraft I, i.e., the ICME direction $\phi_{\rm HM}$ as the result of the HMF method is not the same as the longitudinal separation between the observer O and I, there will be a time delay $t_c \geqslant 0$ when the ICME hits I compared with when the ICME apex is at the same radial distance of I from the Sun. Figure 8(a) visualizes this geometry. We first derive this formula as a "correction" t_c compared with the ICME apex to assess its significance, and will then derive the formula useful for direct calculation of the arrival time $t_{\rm aHM}$. The arrival time correction t_c is a function of the angular separation $\Delta = \phi_{\rm HM} - l_i$ between $\phi_{\rm HM}$ and the heliospheric longitude of I (called l_i), the velocity $V_{\rm HM}$ obtained by the fitting procedure and the radial distance d_i of the in situ spacecraft from the Sun: $t_c(\Delta, V_{\rm HM}, d_i)$. We use all longitudinal angles as such that westward is defined as positive, and the condition $\Delta \in [-\pi/2... + \pi/2]$ is necessary for the spacecraft to be hit by the expanding circular front. In addition, c is defined as the distance the HM apex travels before the HM circle hits the spacecraft I. Applying the law of sines to the triangle indicated in Figure 8(a), we find

$$\frac{(d_i + c)/2}{\sin(\Delta)} = \frac{d_i}{\sin(\pi - 2\Delta)}. \tag{B1}$$

Simple regrouping leads to

$$c = d_i\left(\frac{1}{\cos(\Delta)} - 1\right). \tag{B2}$$

To convert this distance to a time, we assume that the ICME continues to travel with the constant velocity obtained from the fitting procedure ($V_{\rm HM}$) and define $t_c \geqslant 0$ as the arrival time correction,

$$t_c = c/V_{\rm HM}, \tag{B3}$$

$$t_c = \frac{d_i(\cos^{-1}(\Delta) - 1)}{V_{\rm HM}}. \quad \text{(B4)}$$

This can be rewritten as the simple formula

$$t_c\,[\rm hr] = 41555 \times \frac{d_i\,[\rm AU](\cos^{-1}(\Delta) - 1)}{V_{\rm HM}\,[\rm km\ s^{-1}]}, \quad \text{(B5)}$$

with the result t_c in hours and $V_{\rm HM}$ and d_i given in convenient units. Figure 8(b) shows the behavior of $t_c(\Delta)$ for $d_i = 1$ AU and various $V_{\rm HM}$. Obviously, for faster CMEs the arrival time correction decreases, and for a $V_{\rm HM} = 800$ km s^{-1} CME, the arrival time correction is less than 12 hr for $\Delta < 35°$. It might be surprising that Equation (B5) depends on d_i—this is simply because the circle assumed by HM is always attached to the Sun at one end and thus expands while the apex propagates outward.

In summary, to calculate the arrival time of an ICME at a given heliospheric distance d_i and at a longitudinal separation Δ with the HMF method, a correction t_c must be added to the arrival time of the ICME apex:

$$t_{\rm aHM} = t_{\rm 0HM} + \frac{d_i}{V_{\rm HM}} + t_c, \quad \text{(B6)}$$

with $t_{\rm 0HM}$ being the launch time (defined here by $\epsilon(t_{\rm 0HM}) = 0$). This reduces with Equation (B4) to simply

$$t_{\rm aHM} = t_{\rm 0HM} + \frac{d_i}{V_{\rm HM}\cos(\Delta)}. \quad \text{(B7)}$$

This is the final equation for calculating the arrival time of an ICME with the HMF method. From this equation, the elementary result follows that the speed of the ICME flank at a given angle Δ to the ICME apex is simply reduced by a factor $\cos(\Delta)$ for a circular geometry. When comparing the speed $V_{\rm HM}$ as an outcome of the HMF method to in situ measurements of the solar wind bulk speed, the speed $V_{\rm HMI} = V_{\rm HM}\cos(\Delta)$ must be used.

REFERENCES

Bothmer, V., & Schwenn, R. 1998, Ann. Geophys., 16, 1
Bothmer, V., & Zhukov, A. 2006, in Space Weather—Physics and Effects, ed. V. Bothmer & I. A. Daglis (Berlin: Springer), 31
Burlaga, L., Sittler, E., Mariani, F., & Schwenn, R. 1981, J. Geophys. Res., 86, 6673
Cohen, O., Attrill, G. D. R., Manchester, W. B., & Wills-Davey, M. J. 2009, ApJ, 705, 587
Committee on the Societal and Economic Impacts of Severe Space Weather Events 2008, Severe Space Weather Events—Understanding Societal and Economic Impacts: A Workshop Report, Technical Report (Washington, DC: National Academies Press)
Davies, J. A., Harrison, R. A., Rouillard, A. P., et al. 2009, Geophys. Res. Lett., 36, 2102
Davis, C. J., Davies, J. A., Lockwood, M., et al. 2009, Geophys. Res. Lett., 36, 8102
Davis, C. J., de Koning, C. A., Davies, J. A., et al. 2011, Space Weather, 9, 1005
Davis, C. J., Kennedy, J., & Davies, J. A. 2010, Sol. Phys., 263, 209
Eyles, C. J., Harrison, R. A., Davis, C. J., et al. 2009, Sol. Phys., 254, 387
Farrugia, C. J., Burlaga, L. F., Osherovich, V. A., et al. 1993, J. Geophys. Res., 98, 7621
Galvin, A. B., Kistler, L. M., Popecki, M. A., et al. 2008, Space Sci. Rev., 136, 437
Gopalswamy, N., Davila, J. M., St. Cyr, O. C., et al. 2011, J. Atmos. Sol.-Terr. Phys., 73, 658
Gopalswamy, N., Mäkelä, P., Xie, H., Akiyama, S., & Yashiro, S. 2009, J. Geophys. Res. (Space Phys.), 114, A00A22
Gosling, J. T. 1993, J. Geophys. Res., 98, 18937
Howard, R. A., Moses, J. D., Vourlidas, A., et al. 2008, Space Sci. Rev., 136, 67
Howard, R. A., Sheeley, N. R., Jr., Michels, D. J., & Koomen, M. J. 1985, J. Geophys. Res., 90, 8173
Howard, T. A., & Tappin, S. J. 2009a, Space Sci. Rev., 147, 31
Howard, T. A., & Tappin, S. J. 2009b, Space Sci. Rev., 147, 89
Jian, L., Russell, C. T., Luhmann, J. G., & Skoug, R. M. 2006, Sol. Phys., 239, 393
Kahler, S. W., Krucker, S., & Szabo, A. 2011, J. Geophys. Res. (Space Phys.), 116, A01104
Kahler, S. W., & Webb, D. F. 2007, J. Geophys. Res. (Space Phys.), 112, 9103
Kaiser, M. L., Kucera, T. A., Davila, J. M., et al. 2008, Space Sci. Rev., 136, 5
Kienreich, I. W., Temmer, M., & Veronig, A. M. 2009, ApJ, 703, L118
Kilpua, E. K. J., Liewer, P. C., Farrugia, C., et al. 2009, Sol. Phys., 254, 325
Liu, Y., Davies, J. A., Luhmann, J. G., et al. 2010a, ApJ, 710, L82
Liu, Y., Thernisien, A., Luhmann, J. G., et al. 2010b, ApJ, 722, 1762
Lugaz, N. 2010, Sol. Phys., 267, 411
Lugaz, N., Hernandez-Charpak, J. N., Roussev, I. I., et al. 2010, ApJ, 715, 493
Lugaz, N., Roussev, I. I., & Gombosi, T. I. 2011, Adv. Space Res., 48, 292
Lugaz, N., Vourlidas, A., & Roussev, I. I. 2009, Ann. Geophys., 27, 3479
Luhmann, J. G., Curtis, D. W., Schroeder, P., et al. 2008, Space Sci. Rev., 136, 117
Lynch, B. J., Li, Y., Thernisien, A. F. R., et al. 2010, J. Geophys. Res. (Space Phys.), 115, 7106
Miklenic, C., Veronig, A. M., Temmer, M., Möstl, C., & Biernat, H. K. 2011, Sol. Phys., in press
Möstl, C., Farrugia, C. J., Biernat, H. K., et al. 2009a, Sol. Phys., 256, 427
Möstl, C., Farrugia, C. J., Miklenic, C., et al. 2009c, J. Geophys. Res. (Space Phys.), 114, A04102
Möstl, C., Farrugia, C. J., Temmer, M., et al. 2009b, ApJ, 705, L180
Möstl, C., Temmer, M., Rollett, T., et al. 2010, Geophys. Res. Lett., 37, L24103
Nelder, J. A., & Mead, A. 1965, Comput. J., 7, 308
Odstrcil, D. 2003, Adv. Space Res., 32, 497
Patsourakos, S., & Vourlidas, A. 2009, ApJ, 700, L182
Rollett, T., Möstl, C., Temmer, M., et al. 2011, Sol. Phys., submitted
Rouillard, A. P., Davies, J. A., Forsyth, R. J., et al. 2008, Geophys. Res. Lett., 35, 10110
Rouillard, A. P., Davies, J. A., Forsyth, R. J., et al. 2009, J. Geophys. Res. (Space Phys.), 114, 7106
Schmidt, W. K. H., & Bothmer, V. 1996, Adv. Space Res., 17, 369
Sheeley, N. R., Walters, J. H., Wang, Y., & Howard, R. A. 1999, J. Geophys. Res., 104, 24739
Tappin, S. J., & Howard, T. A. 2009, Space Sci. Rev., 147, 55
Temmer, M., Rollett, T., Möstl, C., Veronig, A. M., & Vršnak, B. 2011, ApJ, submitted
Thernisien, A., Vourlidas, A., & Howard, R. A. 2009, Sol. Phys., 256, 111
Tsurutani, B. T., Smith, E. J., Gonzalez, W. D., Tang, F., & Akasofu, S. I. 1988, J. Geophys. Res., 93, 8519
Vourlidas, A., & Howard, R. A. 2006, ApJ, 642, 1216
Williams, A. O., Davies, J. A., Milan, S. E., et al. 2009, Ann. Geophys., 27, 4359
Wood, B. E., & Howard, R. A. 2009, ApJ, 702, 901
Wood, B. E., Howard, R. A., & Socker, D. G. 2010, ApJ, 715, 1524
Yamamoto, T. T., Kataoka, R., & Inoue, S. 2010, ApJ, 710, 456
Zhang, J., Richardson, I. G., Webb, D. F., et al. 2007, J. Geophys. Res. (Space Phys.), 112, 10102
Zhang, T. L., Baumjohann, W., Delva, M., et al. 2006, Planet. Space Sci., 54, 1336